

Detection of Leaking CO₂ Gas With Vegetation Reflectances Measured By a Low-Cost Multispectral Imager

Justin A. Hogan, *Student Member, IEEE*, Joseph A. Shaw, *Senior Member, IEEE*, Rick L. Lawrence, Jennifer L. Lewicki, Laura M. Dobeck, and Lee H. Spangler

Abstract—Multispectral vegetation reflectance measurements were used as an indirect method of sensing CO₂ gas leaking from underground in a controlled release experiment in Bozeman, Montana, USA. The leak location is identified through time-series analysis of the reflectances and the normalized difference vegetation index (NDVI), evaluated at a test location and a control location. Vegetation reflectance changes that correlated with root-level CO₂ exposure were distinguishable from changes attributed to seasonal factors including precipitation, wind, air temperature variation, etc. The NDVI of the vegetation became steadily smaller until saturating approximately twenty days after the beginning of the release. However, before reaching the threshold values, both reflectance and NDVI values changed more rapidly when exposed to elevated CO₂ fluxes.

Index Terms—Environmental management, multispectral imaging, remote monitoring, remote sensing.

I. INTRODUCTION

TO REDUCE atmospheric emissions, carbon capture and sequestration (CCS) is proposed as a means of collecting CO₂ gas generated through industrial and consumer processes and sequestering it to prevent its release into the atmosphere. Proposed methods of sequestration include direct deep-sea injection [1], soil sequestration through improved land use and management practices [2], and geological carbon sequestration, which is the technique of interest in this paper. A diverse technology portfolio is required for the implementation of safe and effective geological sequestration solutions [3]. This includes technology capable of monitoring sequestration site integrity, detecting and signaling leakage should it occur. Early leak detection is crucial to ensuring on-site safety and to minimizing environmental effects. This research focuses primarily on developing and testing remote-sensing leak detection technology for eventual deployment to geological sequestration sites.

Manuscript received August 31, 2011; revised November 23, 2011; accepted April 29, 2012. Date of current version June 28, 2012. This material is based upon work supported by the Department of Energy under award number DE-FE0000397.

J. A. Hogan and J. A. Shaw are with the Electrical and Computer Engineering Department, Montana State University, Bozeman, MT 59717 USA.

R. L. Lawrence is with the Land Resources and Environmental Sciences Department, Montana State University, Bozeman, MT 59717 USA.

J. L. Lewicki is with the U.S. Geological Survey, Menlo Park, CA 94025 USA.

L. M. Dobeck and L. H. Spangler are with the Energy Research Institute, Montana State University, Bozeman, MT 59717 USA.

Color versions of one or more of the figures in this paper are available online at <http://ieeexplore.ieee.org>.

Digital Object Identifier 10.1109/JSTARS.2012.2202880

There are many complementary approaches proposed for monitoring sequestration sites, both directly and indirectly, by observing effects of CO₂ leakages as they are exhibited in various ways. Techniques include *in-situ* infrared gas analyzers, which measure concentrations of CO₂ in a subsurface or near-surface atmosphere by measuring absorption of infrared light [4], tunable differential-absorption laser systems, which measure the light absorption differences between lasers on and off CO₂ absorption features [5], differential absorption LiDAR (DIAL) and Raman LiDAR systems [4], and aerial or ground-based hyperspectral [6] and multispectral [7] imagers. Imaging instruments are able to monitor larger spatial areas than many of the direct measurement techniques. Sequestration projects over large areas may require monitoring over tens to hundreds of square-kilometers [8].

The technique presented in this research used a custom-designed, low-cost multispectral imaging system with sensitivity in red (630–670 nm) and near-infrared (780–820 nm) wavelengths to study the effects on vegetation of CO₂ released from a sub-surface source. The intent is to indirectly detect the presence of CO₂ by observing changes in overlying vegetation. The system was deployed to a controlled sub-surface release facilitated by the ZERO Emissions Research and Technology Center (ZERT) in Bozeman, Montana in the summer of 2010. The annual release is an opportunity for scientists and engineers from all over the country to conduct near-surface monitoring experiments in an effort to better understand the behavior of CO₂ leaking from an underground source, study the effects of CO₂ on vegetation and acquire important knowledge regarding how CO₂ interacts with the environment and how its presence is best detected. Proof-of-principle experiments were conducted during previous release experiments in 2007 and 2008 using a commercial multispectral imager [7], and the results here use a newly designed imager to provide confirmation of the earlier results while also adding refined spatial and statistical analysis. This paper discusses the justification for a near-surface imaging approach to site monitoring, a brief overview of the imaging system that was deployed to the 2010 ZERT experiment, a summary of the data collected, and results of the data analysis.

II. METHODS

A. Vegetation Reflectance Spectral Imaging

Reflectance properties of vegetation are determined by a variety of factors, including leaf age, water content, cell structure, pigment content, surface properties, and angle of incidence

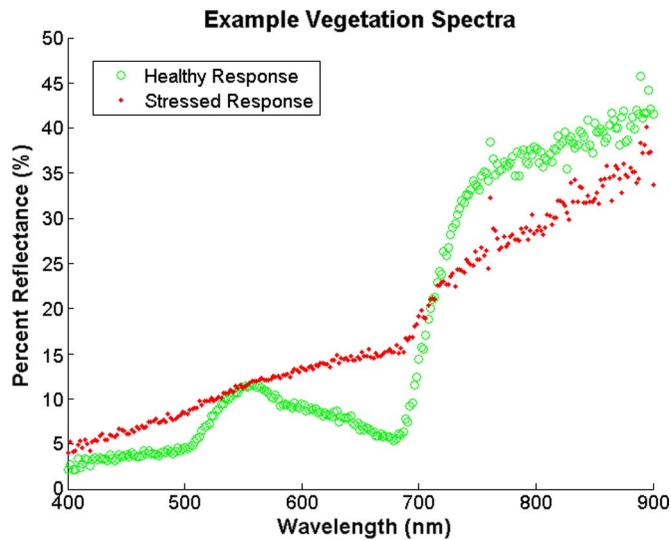


Fig. 1. Example vegetation reflectance spectra acquired by a handheld spectrometer.

of incoming light [9]. Healthy vegetation exhibits significantly higher reflectance of near-infrared light than visible light. The sharp increase in vegetation reflectance, which occurs rapidly in the spectral vicinity of 700 nm, is known as the “red edge” and is a result of chlorophyll reflectance. Example reflectance spectra for healthy and unhealthy vegetation are shown in Fig. 1. These spectra were measured with a hand-held spectrometer at the “control” and “hot spot” regions of the vegetation test area late in the study during summer 2010.

As indicated in (1), the Normalized Difference Vegetation Index (NDVI) uses the near-infrared and red reflectances, ρ_{NIR} and ρ_{Red} , respectively, to provide a numerical estimate of vegetation health (note that each channel’s digital number is corrected for dark signal and angle-dependent optics response before being converted to the corresponding reflectance). As plants become stressed and die, seasonally or otherwise, an increase in red reflectance and a decrease in near-infrared reflectance results in a flattening of the reflectance spectrum and a corresponding reduction of the NDVI, which is interpreted as a decrease in vegetation amount, health, or vigor.

$$\text{NDVI} = \frac{\rho_{\text{NIR}} - \rho_{\text{RED}}}{\rho_{\text{NIR}} + \rho_{\text{RED}}} \quad (1)$$

Although modest increases in CO_2 concentration in the air can act as a nutrient to plants [10], increased concentration of CO_2 in the soil displaces oxygen around the roots, causing plant stress through asphyxiation [11], [12] or soil acidification [13]. This plant stress can be detected as changes in the reflectances and the NDVI. The basis for this study is that time-series trends in red reflectance, near-infrared reflectance and NDVI can be used to indirectly detect the presence of abnormally high concentrations of root-level CO_2 by observing the resultant stress as manifested spectrally by the vegetation.

Rather than relying on reflectances or NDVI alone, the statistical analysis of our data used both reflectances and the NDVI together because the NDVI is an interaction term that models the interaction of the two band reflectances [14]. To model the

main effects of the two spectral regions, it is necessary to include the individual band reflectances in the statistical analysis. Previous research, however, indicates that there might also be an interaction between the bands, so that including NDVI as an interaction term is appropriate as well. The regression analysis indicates the appropriateness of each band and interaction in the final model.

One limitation of this method is that it cannot uniquely identify the specific cause of observed stress. In fact, previous studies have shown that this method can detect stress caused by increased CO_2 flux or hail storms, as well as short-term increases in vegetation health resulting from rapid increases in soil moisture from heavy rains [7]. However, these other variations act with essentially equal influence throughout our study region. Furthermore, the vegetation type was quite consistent through the field where our study was conducted. Although we show only results from 2010 in this paper, similar results have been obtained with similar imaging systems over a four-year period (2007–2011), including vastly different temperature and moisture patterns [7], [15].

The primary advantage of this method is that it can identify areas of a field that warrant direct inspection by identifying areas of vegetation that exhibit significantly different reflectance values than surrounding vegetation. This serves to reduce the extent of required *in-situ* monitoring by leveraging the wide-area coverage of an imaging system.

The imaging system used to collect the data presented in this paper was a second-generation system designed to consume less power and be more compact at lower cost than the original instrument while maintaining similar spectral sensitivity and field-of-view. A Pixelink PL-B741U camera model was chosen for use in the system, which featured a 1280-by-1024 pixel monochrome CMOS sensor with high red and near-infrared sensitivity, a USB control interface, and C-mount lens attachment threads. A Tamron 6.5-mm C-mount lens was chosen as the primary optical element because of its short focal length, which provided a good start to achieving the desired 45° field-of-view. Spectral channel selection was achieved using a Thorlabs FW102B filter wheel populated with one-inch circular interference filters. Each filter had a 40-nm full-width half-maximum passband centered at 650 nm for the red and 800 nm for the near-infrared channel. Reduction of the center wavelength of interference filters for non-normal incidence angles prevented placement of the filter wheel in front of the Tamron lens mounted directly to the camera. Space to insert the filter wheel between the Tamron lens and the camera body was created by using field lenses to pseudo-collimate and relay light through the filters and a triplet behind the filters to re-image the light onto the camera detector. Inaccurate estimates of ray angles exiting the Tamron lens resulted in a trade-off of reduced image resolution for required field-of-view. The details of the design and operation of this imaging system are reported elsewhere [16].

B. Experiment Overview

The imager was deployed at the ZERT field site, located just west of the MSU campus in Bozeman, Montana. The site is an approximately 0.35 square-km, nominally flat pasture



Fig. 2. Three CO₂ hot spots near the end of the 2009 release (long after they were detectable with multispectral imaging), along with equipment situated above the buried release pipe.

consisting of a variety of vegetation [15]. Vegetation includes western salsify, dandelion, Canada thistle, alfalfa, birdsfoot trefoil, clover, lupine, quackgrass, orchard grass, and Kentucky bluegrass [17]. CO₂ is released from an on-site storage tank into a 100-m horizontal injection well buried approximately 1.8-m below the surface. The release pipe is divided into six zones, each with its own release rate control mechanism. CO₂ surface flux measurements taken during previous experiments have shown that the gas does not exit the surface uniformly along the length of the pipe; rather, several localized regions of high flux are observed [15]. These regions are called “hot spots.” By the end of a release, the CO₂ hot spots are visible as nominally circular patches of completely dead vegetation (but the imager detects their onset long before they are obvious to the eye). Fig. 2 shows these hot spots observed near the end of the 2009 release.

During the 2010 release experiment, extending from 19 July to 15 August, 2010, the multi-spectral imager was deployed to a specific region of the test field known as the plant block, a 400-m² area of vegetation that is bisected by the buried release pipe, cordoned off from the rest of the field, and reserved for plant research. For this release, the vegetation test area was not mown. Fig. 3 shows a general layout of the plant block.

The instrument was housed atop a 3-m tall scaffold and viewed the vegetation test area at a downward angle of 45°. The scaffolding was offset approximately three meters from the pipe, with the imagers situated such that the release pipe ran horizontally through the image. This setup provided enough height for the imager to view vegetation from the pipe out to the edge of the test area. This field-of-view purposely included control vegetation well removed from the release pipe representing vegetation unaffected by released CO₂. The field-of-view also included a portion of the observed CO₂ hot spot, which displayed the most dramatic effects of the released CO₂ on the vegetation. Fig. 4 shows the instrument deployed atop the scaffolding, along with other sensors.

The imaging system was designed to have an automated data acquisition process that relies on a known-reflectance calibration target placed in the field-of-view. The target used

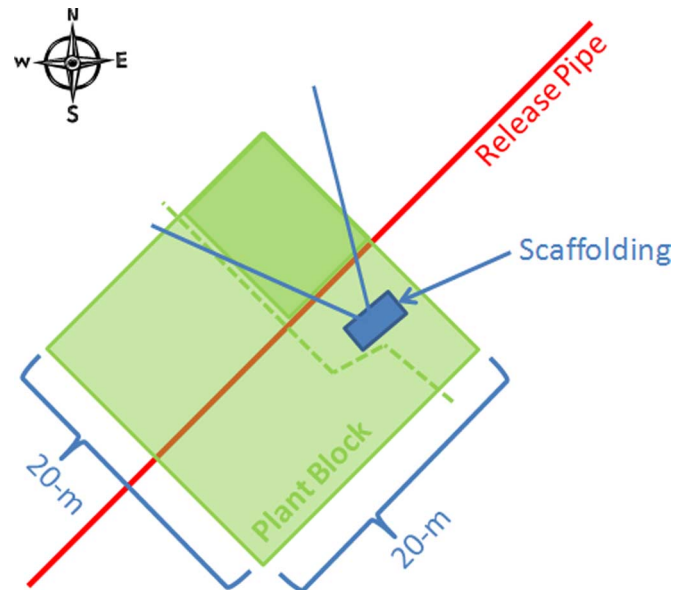


Fig. 3. Plant block layout including vegetation test area dimensions, walking path through test area, instrument housing scaffolding, release pipe location, and nominal instrument field-of-view.



Fig. 4. Multi-spectral imager mounted along with other sensors on scaffolding at the ZERT test site. The imager views the scene through the left window (from the observer’s perspective) of the white box.

was a 12-inch square reflectance calibration panel made of Spectralon© material, which is a Lambertian surface with flat reflectance values across much of the visible and near-infrared spectrum. In data acquisition, this panel was used as a feedback mechanism in an exposure-time control loop which adjusted the camera’s integration time until the average pixel value of the reflectance panel is between 240 and 250 digital numbers. This maximized the dynamic range of the measurements by utilizing as much of the 8-bit values as possible. In post processing, the reflectance panel was used to calculate a calibrated reflectance

image using the known red and near-infrared reflectance values of 0.9894 and 0.9896, respectively. The calibrated images were calculated as the ratio of each pixel to the average value of the calibration panel multiplied by the known panel reflectance values of the respective channels. The calibrated images were subsequently used in the calculation of an NDVI image.

Ground-truth data were provided by measuring soil CO₂ fluxes with an accumulation chamber method, with samples spaced by 5 m along the well and additional samples spaced by 2.5 m along lines transverse to the well at 10-m interline spacing [18]. During the 2010 experiment, fluxes were measured for the full grid on 27 and 29 July near the middle of the release, and at 1-m spacing along the surface trace of the well on 28 July. The average of the 27 and 29 July CO₂ flux measurements was 29.4 g/(m²d) far from the release pipe in the upper-left region of the vegetation images analyzed as control region and 91.7 g/(m²d) near the edge of the hot spot, in the image region that was analyzed as “hot spot” data. The background CO₂ flux in locations far from the release pipe varied between approximately 15 and 20 g/(m²d). Therefore, our “control” analysis region exhibited CO₂ flux approximately fifty percent higher than background, while the “hot spot” analysis region exhibited CO₂ flux nearly five times background and three times the “control” value. While this flux difference cannot rule out the existence of other stressors, it provides important confirmation that there was higher CO₂ flux in regions where our imaging system detected higher vegetation stress.

III. DATA AND ANALYSIS

The 2010 release spanned 27 days, from July 19 to August 15, with a CO₂ flow rate of 0.15 tons/day. Data were collected for 25 of the 27 days during which CO₂ was released. Data were collected for seven days prior to the start of the release to provide baseline measurements of the vegetation while it was seasonally healthy. Data collection continued for 14 days after the release to observe how the vegetation responded. By the mid-point of the release there were several discernible regions of stress within the test area. Around the hot spot, areas stressed by large amounts of foot traffic also were present, but were not included in the analysis.

The data were extensively filtered to reduce the number of images to a workable set. This included removal of images with people in the test area, occlusion of or debris on the calibration panel, rain on the observation window, over- or under-exposure, etc. Images were acquired every six minutes between 9 AM and 4 PM each day. An analysis to determine if there was discernible fluctuation of reflectance with changing solar elevation angle found no significant trends, but it led to the observation that measurements taken in the morning hours exhibited a greater degree of variability than afternoon measurements. This variability was not observed for every day examined, which allowed illumination geometry to be eliminated as the source of the behavior. We hypothesize that occasional overnight dew formation on the canopy resulted in higher variability of the measurements in the morning hours. As a result, morning images were discarded and a single daily average image for red reflectance, near-infrared reflectance, and NDVI was calculated

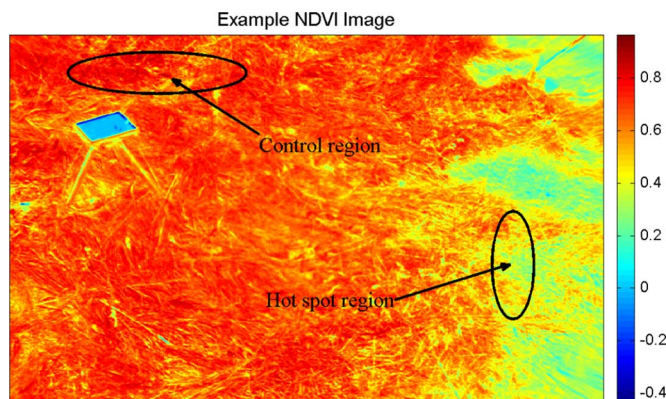


Fig. 5. Example NDVI image labeled to indicate the approximate control and hot spot regions used in data processing. Some of the regions of extremely high vegetation stress along the right side of the image are a result of human foot traffic. This image covers the area enclosed approximately by the blue lines marking the imager's field of view in Fig. 3.

using afternoon data. This averaging also avoided times during which the shadow of the instruments and housing was cast into the field-of-view.

The data were analyzed statistically in two distinct regions: a control region located approximately 9 m from the buried release pipe, and a hot spot region near the release pipe. The hot spot region was known from previous studies [7], [15], [16] to experience significantly higher CO₂ fluxes than the control region. As explained at the end of Section II, flux measurements made during late July 2010, in the midst of this study, showed at least three times higher CO₂ flux in the hot spot analysis region relative to the control region. The pixels chosen for inclusion in the analyzed image regions were well within the boundaries of vegetation that was never subjected to foot traffic or other causes of vegetation stress. Fig. 5 shows an example NDVI image identifying the approximate hot spot and control regions used for data processing. In the subsequent statistical analysis, time-series trends of the reflectance and NDVI data from these two regions were compared, as detailed next.

In the analysis, time was represented as ‘experiment day’ with day one corresponding to the first day of acquired data. Simple linear regressions of experiment day versus red reflectance, near-infrared reflectance and NDVI were calculated. Though experiment day was used as the response variable in each of the regressions, the data were plotted with experiment day as the explanatory variable, as this visual representation is more intuitive. Equation (2) shows the model used for the red reflectance analysis,

$$\text{Day} = \beta_0 + \beta_1 \text{RED} + \beta_2 \text{HS} + \beta_3 \text{HS}, \quad (2)$$

where *HS* is a categorical variable used to distinguish hot spot vegetation from control vegetation data. This equation was also used for the near-infrared and NDVI data with the variable *RED* replaced with the appropriate data series. As the data represent a small segment of a long-run data set, analysis was performed to adjust model parameters’ significance values for the effects of serial correlation. Though it was present in the data, it was not found to change the statistical significance of any of the regressions.

TABLE I
2010 RED REFLECTANCE REGRESSION SUMMARY

Day vs. Red Reflectance Regression Summary $R^2=0.87$					
Description	Parameter	Estimate	Standard Error	t-statistic	Two-sided p-value
Control Intercept	β_0	-21.957	2.868	-7.657	< 0.01
Control Red Slope	β_1	435.943	24.762	17.605	< 0.01
Hotspot Intercept	β_2	-19.080	5.045	-3.782	< 0.01
Hotspot Red Slope	β_3	-29.924	34.793	-0.860	0.39

TABLE II
2010 NEAR-INFRARED REFLECTANCE REGRESSION SUMMARY

Day vs. Near-Infrared Reflectance Regression Summary $R^2=0.58$					
Description	Parameter	Estimate	Standard Error	t-statistic	Two-sided p-value
Control Intercept	β_0	121.41	11.49	10.569	< 0.01
Control NIR Slope	β_1	-168.35	20.30	-8.291	< 0.01
Hotspot Intercept	β_2	15.14	18.88	0.802	0.42
Hotspot NIR Slope	β_3	-77.70	39.14	-1.985	0.05

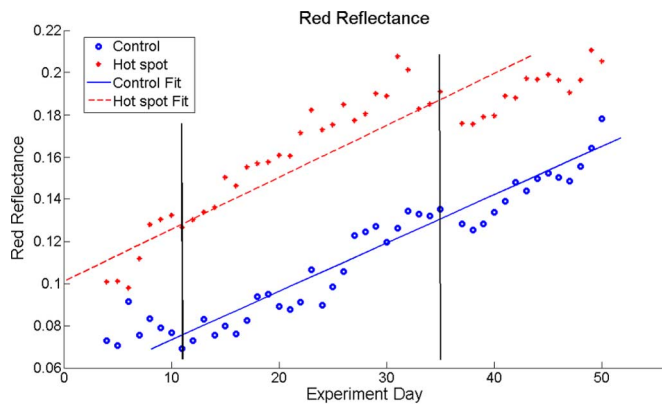


Fig. 6. Time-series plot of red reflectance data along with regression lines for both control and hot spot data. The beginning and end of the release experiment are marked by the solid black vertical lines.

Fig. 6 shows the red reflectance data set along with the corresponding regression lines and Table I shows the numerical regression results. In this and subsequent figures that show reflectance and NDVI data, the measurement error bars are of comparable size to the plot symbols. The small errors arise because each point on the graph represents a spatial average over the control or hot spot region, as well as a temporal average over all valid images obtained on a given day (i.e., one point represents the average for a chosen region for a specific day). Therefore, day-to-day fluctuations of reflectances or NDVI are believed to represent real fluctuations in the vegetation, arising from changes in sunlight, moisture, and so forth. In interpreting the regression results in Table I and the subsequent tables, note that t-statistic values greater than 2 and p-values less than 0.05 are considered significant.

As expected, red reflectance increased throughout the experiment as the vegetation experienced natural seasonal stress. A small initial offset in red reflectance between the two regions

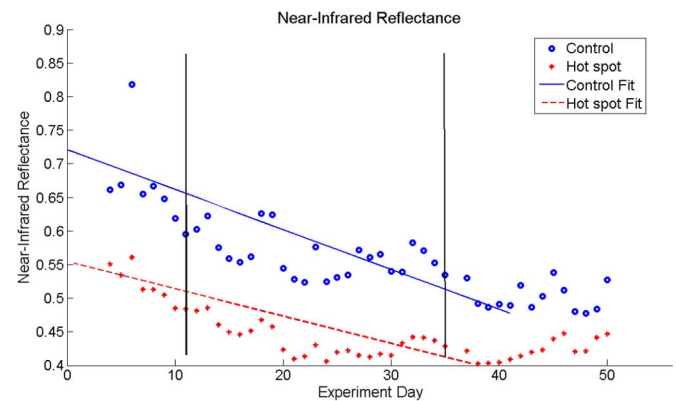


Fig. 7. Time-series plot of near-infrared reflectance data along with regression lines for both control and hot spot vegetation. The beginning and end of the release experiment are marked by the solid black vertical lines.

was observed. Residual effects from a release in June 2010 were considered as a potential cause of the initial offset. The offset was found to be statistically significant as evidenced by the p-value of the β_2 parameter in Table I. It was expected that a statistically significant difference in slopes would be observed as well, but that was not the case when considering the full data series. These data did show a visibly sharper increase in red reflectance for the hot spot vegetation during the release and prior to reaching a threshold reflectance around 20%. The fact that the reflectance reached a maximum value and flattened out helped explain the lack of a significantly different slope between hot spot and control vegetation in this model. At the end of the experiment, the control vegetation red reflectance was still increasing and never reached the same level as the hot spot vegetation.

Near-infrared reflectance followed a decreasing trend throughout the experiment. This, combined with the increasing

TABLE III
2010 NDVI REGRESSION SUMMARY

Day vs. NDVI Regression Summary $R^2=0.88$					
Description	Parameter	Estimate	Standard Error	t-statistic	Two-sided p-value
Control Intercept	β_0	120.447	4.961	24.277	< 0.01
Control NDVI Slope	β_1	-140.719	7.379	-19.071	< 0.01
Hotspot Intercept	β_2	-38.761	5.969	-6.493	< 0.01
Hotspot NDVI Slope	β_3	20.666	10.235	2.019	0.05

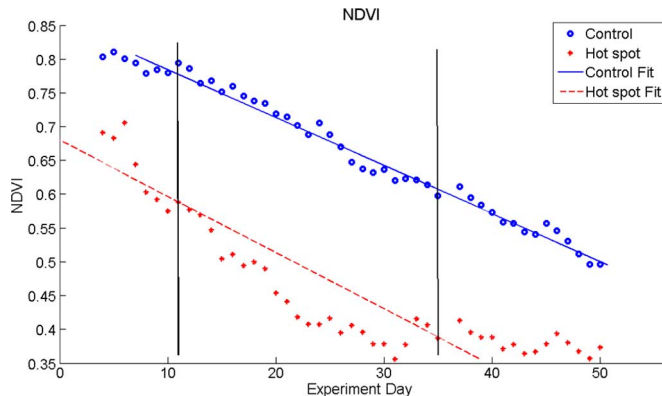


Fig. 8. Time-series plot of the NDVI data along with regression lines for both control and hot spot vegetation. The beginning and end of the release experiment are marked by the vertical lines.

red reflectance, demonstrated the previously mentioned flattening of the reflectance spectrum as vegetation becomes stressed. The time-series data for control and hot spot vegetation are shown in Fig. 7 and the regression results are summarized in Table II.

The analysis from this model showed little statistical evidence of a difference in response between the hot spot and control vegetation. However, this does not mean that there was no difference. Rather, it suggests that a linear model is not ideal for explaining the behavior of the data, which is evidenced by the relatively low R^2 value of 0.58. However, there are still important qualitative observations which can be made. The hot spot vegetation appeared to reach a low-threshold value of approximately 40% near-infrared reflectance around experiment day 20, with some recovery observed following the end of the release. By the end of the deployment, the control and hot spot near-infrared reflectance measurements were closer than the initial offset, but had not completely converged. The trends in these data were not as strong as in the red reflectance data, but a threshold-type behavior is similarly observed.

The NDVI data more clearly demonstrated the response difference between the two vegetation regions. The NDVI values were offset between the two regions at the start of the release, presumably a result of the earlier mini-release mentioned previously. Fig. 8 shows a time-series plot of the NDVI data for the control and hot spot vegetation, along with regression lines for each. The regression results are summarized in Table III.

All model parameters in the NDVI regression were significant. The hot spot vegetation was found to start the experiment

in a less healthy condition and decrease in health more rapidly than the control vegetation. Visually, it was seen that the NDVI reached a threshold value between 0.35 and 0.40 by experiment day 30, about which it oscillated through the remainder of the deployment. The control vegetation continued a fairly linear decline throughout the entire deployment and never reached a threshold value. Taken to represent vegetation health, these data showed a fairly monotonic decline in health for the control vegetation, which was dominated by seasonal factors shared with the hot spot vegetation. In addition to seasonal stresses, the hot spot NDVI data reflected the stress associated with the injected CO_2 .

A full model including both reflectance data and NDVI was analyzed and reduced using a forward/backward stepwise procedure. This process removed explanatory variables whose regression coefficients were insignificant at a 0.05 significance level. The generalized model used for analyzing the data is shown in (3).

$$\text{Day} = \beta_0 + \beta_1 \text{RED} + \beta_2 \text{NIR} + \beta_3 \text{NDVI} + \beta_4 \text{HS} + \beta_5 \text{RED} \cdot \text{HS} + \beta_6 \text{NIR} \cdot \text{HS} + \beta_7 \text{NDVI} \cdot \text{HS} \quad (3)$$

The variable selection process yielded the results shown in Table IV. The residuals for the multiple regression model are plotted in Fig. 9.

The variables excluded from the model were red reflectance and near-infrared reflectance for the control vegetation, and an additive initial offset term for the hot spot vegetation. The red reflectance, near-infrared reflectance, and NDVI were all important in explaining the variability for the hot spot while NDVI alone was sufficient for the control vegetation. After accounting for NDVI in the control data, red and near-infrared reflectance did not provide significant explanation of remaining variability. The results of this model showed a notable difference in red reflectance, near-infrared reflectance, and NDVI trends for vegetation exposed to high soil CO_2 concentrations. Although the reflectance and NDVI data exhibit a threshold behavior near day 30 of the analysis, the entire data set is used in the analysis to illustrate that the method can be used to detect CO_2 -affected vegetation without isolating specific subsets of data. A more complete analysis and discussion of the data set is available elsewhere [16].

IV. CONCLUSIONS

During this experiment, vegetation reflectance changes that correlated with root-level CO_2 exposure were distinguishable

TABLE IV
2010 REDUCED MODEL REGRESSION SUMMARY

Reduced Model Summary R ² =0.91					
Description	Parameter	Estimate	Standard Error	t-statistic	Two-sided p-value
Intercept	β_0	120.680	4.217	28.618	< 0.01
Control NDVI Slope	β_3	-141.062	6.272	-22.491	< 0.01
Hot spot Red Slope	β_5	-501.379	59.232	-8.465	< 0.01
Hot spot NIR Slope	β_6	404.848	59.118	6.848	< 0.01
Hot spot NDVI Slope	β_7	-276.052	37.505	-7.360	< 0.01

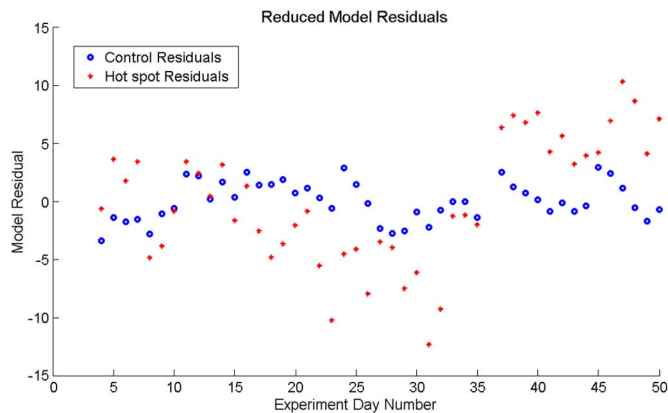


Fig. 9. Time-series plot of the residuals of the multiple regression model, which considers red reflectance, near-infrared reflectance, and NDVI.

from changes attributed to seasonal factors including precipitation, wind, temperature variation, soil conditions, etc. Important observations that can be taken from this study include the threshold behavior of NDVI and the constituent reflectances, and more rapid reflectance and NDVI changes during exposure to CO₂ before reaching the threshold.

We note that different results may be obtained if this method is applied in an area with different plant types or with vastly differing conditions. Furthermore, the method is obviously only useful during an active growing season. The method lacks the ability to identify the exact cause of vegetation stress, but it is useful for identifying regions of abnormally high stress, which warrant further investigation with in-situ measurements.

This study has shown that statistically significant results can be obtained, which identify regions of high CO₂ flux through time-series analysis of measurements of vegetation reflectance made with a very low-cost, compact imaging system. We note that in this study it was necessary to deploy a calibration panel so the data could be converted to reflectance values before calculating the NDVI, but in general this is not required. Our use of 8-bit images in this study made it necessary to adjust the camera's integration time as solar irradiance changed with time of day, cloud conditions, etc., but by simply using the higher bit depth available from the camera, the need for a reflectance calibration can be eliminated and the analysis can make direct use of the digital numbers from the images (after necessary correction for angle- and wavelength-dependent camera response, etc.). Related to this, one of the potentially important findings of this study is that there was no time of day that was better

than others, once dew had disappeared from the vegetation. The numerical analysis presented here, using reflectance and NDVI data, is preliminary to the development of automated leak detection algorithms capable of identifying suspected leak areas in the absence of *a priori* leak location information.

ACKNOWLEDGMENT

This report was prepared as an account of work sponsored by an agency of the United States Government. Neither the United States Government nor any agency thereof, nor any of their employees, makes any warranty, express or implied, or assumes any legal liability or responsibility for the accuracy, completeness, or usefulness of any information, apparatus, product, or process disclosed, or represents that its use would not infringe privately owned rights. Reference herein to any specific commercial product, process, or service by trade name, trademark, manufacturer, or otherwise does not necessarily constitute or imply its endorsement, recommendation, or favoring by the United States Government or any agency thereof. The views and opinions of authors expressed herein do not necessarily state or reflect those of the United States Government or any agency thereof.

REFERENCES

- [1] C. Marchetti, "On geoengineering and the CO₂ problem," *Climatic Change*, vol. 1, no. 1, pp. 59–68, 1977.
- [2] R. Lal, "Soil carbon sequestration to mitigate climate change," *Geoderma*, vol. 123, no. 1–2, pp. 1–22, 2004.
- [3] IPCC, Carbon Dioxide Capture and Storage 2005 [Online]. Available: http://www.ipcc.ch/publications_and_data/publications_and_data_reports.shtml
- [4] C. M. Oldenburg, J. L. Lewicki, and R. P. Hepple, Near-Surface Monitoring Strategies for Geologic Carbon Dioxide Storage Verification Lawrence Berkeley National Laboratory report LBNL-54089, 2003 [Online]. Available: <http://escholarship.org/uc/item/1cg241jb>
- [5] J. L. Barr, S. D. Humphries, A. R. Nehrir, K. S. Repasky, L. M. Dobeck, J. L. Carlsten, and L. H. Spangler, "Laser-based carbon dioxide monitoring instrument testing during a 30-day controlled underground carbon release field experiment," *Int. J. Greenhouse Gas Control*, vol. 5, no. 1, pp. 138–145, 2010.
- [6] C. J. Keith, K. S. Repasky, R. L. Lawrence, S. C. Jay, and J. L. Carlsten, "Monitoring effects of a controlled subsurface carbon dioxide release on vegetation using a hyperspectral imager," *Int. J. Greenhouse Gas Control*, vol. 3, pp. 626–632, 2009.
- [7] J. H. Rouse, J. A. Shaw, R. L. Lawrence, J. L. Lewicki, L. M. Dobeck, K. S. Repasky, and L. H. Spangler, "Multi-spectral imaging of vegetation for detecting CO₂ leaking from Underground," *Environ. Earth Sci.*, vol. 60, pp. 313–323, 2010.
- [8] Geologic CO₂ Sequestration Research at the USGS [Online]. Available: http://energy.er.usgs.gov/health_environment/co2_sequestration/co2_illustrations.html
- [9] E. A. Walter-Shea and J. M. Norman, "Leaf optical properties," *Photon-Vegetation Interactions*. ch. 8, 1991, pp. 230–250.

- [10] B. A. Kimball, J. R. Mauney, F. S. Nakayama, and S. B. Idso, "Effects of increasing atmospheric CO₂ on vegetation," *Plant Ecology*, vol. 104–105, no. 1, pp. 65–75, 1993.
- [11] J. Qi, J. D. Marshall, and K. G. Matson, "High soil carbon dioxide concentrations inhibit root respiration of Douglas Fir," *New Phytologist*, vol. 128, no. 3, pp. 435–442, 1994.
- [12] I. Macek, H. Pfanz, V. Francetic, F. Batik, and D. Vodnik, "Root respiration response to high CO₂ concentrations in plants from natural CO₂ springs," *Environmental and Experimental Botany*, vol. 54, no. 1, pp. 90–99, 2005.
- [13] K. A. McGee and T. M. Gerlach, "Annual cycle of magmatic CO₂ in a tree-kill soil at Mammoth Mountain, California: Implications for soil acidification," *Geology*, vol. 26, no. 5, pp. 463–466, 1998.
- [14] R. L. Lawrence and W. J. Ripple, "Comparisons among vegetation indices and bandwise regression in a highly disturbed, heterogeneous landscape: Mount St. Helens, Washington," *Remote Sensing of Environment*, vol. 64, no. 1, pp. 91–102, 1998.
- [15] L. H. Spangler, L. M. Dobeck, K. S. Repasky, A. R. Nehrir, S. D. Humphries, J. L. Barr, C. J. Keith, J. A. Shaw, J. H. Rouse, A. B. Cunningham, S. M. Benson, C. M. Oldenburg, J. L. Lewicki, A. W. Wells, J. R. Diehl, B. R. Strazisar, J. E. Fessenden, T. A. Rahn, J. E. Amonette, J. L. Barr, W. L. Pickles, J. D. Jacobson, E. A. Silver, E. J. Male, H. W. Rauch, K. S. Gullickson, R. Trautz, Y. Kharaka, J. Birkholzer, and L. Wielopolski, "A shallow subsurface controlled release facility in Bozeman, Montana, USA, for testing near surface CO₂ detection techniques," *Environmental Earth Sciences*, vol. 60, no. 2, pp. 227–239, 2010.
- [16] J. A. Hogan, "Multi-Spectral Imaging of Vegetation for CO₂ leak detection" M.S. Thesis, Department of Electrical and Computer Engineering, Montana State University, , 2011 [Online]. Available: <http://etd.lib.montana.edu/etd/view/item.php?id=1255>
- [17] E. J. Male, W. L. Pickles, E. A. Silver, G. D. Hoffmann, J. Lewicki, M. Apple, K. Repasky, and E. A. Burton, "Using hyperspectral plant signatures for CO₂ leak detection during the 2008 ZERT CO₂ sequestration field experiment in Bozeman, Montana," *Environmental Earth Sciences*, vol. 60, no. 2, pp. 251–261, 2010.
- [18] J. L. Lewicki, G. E. Hilley, L. Dobeck, and L. Spangler, "Dynamics of CO₂ fluxes and concentrations during a shallow subsurface CO₂ release," *Environmental Earth Sciences*, vol. 60, no. 2, pp. 285–297, 2010.



Justin A. Hogan received a Bachelor's degree in electrical engineering with a supplemental major in applied mathematics from New Mexico State University in Las Cruces, New Mexico, USA in 2008. He received a Master of Science degree in electrical engineering from Montana State University in Bozeman, Montana, USA in 2011.

He is currently a doctoral student in the electrical and computer engineering department at Montana State University where he works with the radiation tolerant computing group as a graduate research assistant. His research interests include embedded system design and development, radiation tolerant computing system research, and FPGA system design.



Joseph A. Shaw (S'84–M'90–SM'04) received the B.S. degree in electrical engineering from the University of Alaska, Fairbanks, the M.S. degree in electrical engineering from the University of Utah, Salt Lake City, and the M.S. and Ph.D. degrees in optical sciences from the University of Arizona, Tucson, in 1987, 1989, 1994, and 1996, respectively.

He was an Electro-optical Engineer at the National Oceanic and Atmospheric Administration (NOAA) Environmental Technology Laboratory, Boulder, CO, from 1989 to 2001, where he developed infrared spectro-radiometers and laser sensors for studying the Earth's atmosphere and oceans. In 2001, he joined the electrical and computer engineering faculty at Montana State University, Bozeman, where he is now Professor and Director of the Optical Technology Center. His current research is in polarimetric and radiometric imaging and laser remote sensing.

Dr. Shaw is a Fellow of the Optical Society of America (OSA), a Fellow of the International Society of Optics and Photonics (SPIE), and a member of the

American Geophysical Union (AGU). Professional recognition of his contributions to optical remote sensing science, engineering, and education include the Presidential Early Career Award for Scientists and Engineers (PECASE), the Vaisala Award from the World Meteorological Organization, and the Cox Family Award for Excellence in Scholarship and Teaching at Montana State University.



Rick L. Lawrence received a B.A. in political science from Claremont McKenna College, Claremont, California, J.D. from Columbia University School of Law, New York, New York, and M.S. and Ph.D. in forest resources from Oregon State University, Corvallis, Oregon, in 1976, 1979, 1995, and 1998, respectively.

He practiced law from 1979 to 1993 with the law firms or Hughes Hubbard & Reed, Adams, Duque, and Hazeltine, and LeBoeuf Lamb Leiby & McCrea. He joined the Land Resources and Environmental Sciences faculty at Montana State University, Bozeman, where is now Professor and Director of the Spatial Sciences Center. His research spans a wide range of applications related to natural resource management, from carbon sequestration, to crop and range issues, to forest and wildlife. He also has a strong interest in algorithm development for classification of remotely sensed imagery, specializing in classification tree analysis and its variants.

Dr. Lawrence is member of the American Society of Photogrammetry and Remote Sensing, the Society of American Foresters, the American Geophysical Union, and the California Bar Association (inactive).



Jennifer L. Lewicki received the B.A. degree in geology from Hamilton College, Clinton, the M.S. degree in geology from Arizona State University, Tempe, and the Ph.D. degree in geosciences from the Pennsylvania State University, University Park, in 1994, 1997, and 2002, respectively.

She was Postdoctoral Fellow at the University of South Florida, Tampa, FL, from 2002 to 2003 and a Postdoctoral Fellow and Geological Scientist at Lawrence Berkeley National Laboratory, Berkeley, CA from 2003 to 2012. She is currently a Research

Geologist at the U.S. Geological Survey, Menlo Park, CA. Her research is in volcanic and geothermal degassing and fluid geochemistry and near-surface monitoring of geologic carbon sequestration sites.

Dr. Lewicki is a member of the American Geophysical Union.



Laura M. Dobeck received a B.S. degree in chemistry from the University of Wisconsin-Madison in 1991, and M.S. and Ph. D. degrees in physical chemistry from Cornell University in Ithaca, New York in 1994 and 1999, respectively.

She has studied reaction dynamics of small molecules in the gas phase using laser spectroscopy and electron transfer in the solution phase with ultrafast laser systems. Her current interests include studying the transport of CO₂ in the near ground surface and testing and evaluating surface and near-subsurface monitoring techniques to be applied to geological carbon dioxide sequestration. She currently serves as the field site manager for the ZERT shallow subsurface CO₂ controlled release facility at Montana State University-Bozeman.

Dr. Dobeck is a member of the American Geophysical Union (AGU).

Lee H. Spangler received a B.A. degree at Washington & Jefferson College in 1980 and a Ph.D. in Physical Chemistry at the University of Pittsburgh in 1985.

He was a postdoctoral researcher at the Los Alamos National Laboratory from 1985 to 1987. He joined the Chemistry faculty at Montana State University in 1987, where he now serves as the Director of the Energy Research Institute and Associate Vice President for Research.